Uncooled Infrared Detectors Using Gallium Nitride on Silicon Micromechanical Resonators

Vikrant J. Gokhale, *Student Member, IEEE*, and Mina Rais-Zadeh, *Senior Member, IEEE*

***Abstract*— This paper presents the analysis, design, fabrication, and the first measured results demonstrating the use of gallium nitride (GaN)-based micromechanical resonator arrays as high-sensitivity, low-noise infrared (IR) detectors. The IR sensing mechanism is based on monitoring the change in the resonance frequency of the resonators upon near IR radiation. The resonators are characterized for their RF and thermal performance and exhibit a radiant responsivity of 1.68%/W, thermal time constant on the order of 556 μs, and an average IR responsivity of -1.5% when compared with a reference resonator, for a 100 mK radiation-induced temperature rise. An analysis of the design of the devices is presented as a path toward better design, specifically, for low thermal noise equivalent temperature difference in the long wavelength IR spectrum. [2013-0190]**

***Index Terms*— Infrared sensor, uncooled IR detectors, micromachined, NETD, resonators, thermal sensors.**

I. Introduction

IN RECENT years, there has been a growing interest in high-precision infrared (IR) detectors for applications ranging from military, defense and security to automotive and consumer markets [1]–[3]. There are two main types of IR detectors: photonic detectors and thermal detectors. Photonic detectors depend on band-gap transitions due to photonic excitation in detector materials. These detectors work best at low temperatures, although efforts are being made to develop high operating temperature photonic detectors [2]. Thermal detectors, on the other hand, depend on the conversion of incident radiation to heat, which is subsequently transduced into an electrical signal. Thermal detectors typically do not require cooling and are designed to work at 300 K and higher. In the last couple of decades, there has been a large surge in the number of solutions that use uncooled detectors, primarily due to the fact that cooled sensors, even though they have enhanced sensitivity, require a bulky cooling/refrigeration unit that consumes both space and power. The high cost of cooled detectors also makes them unattractive to the growing automotive and consumer market.

Most successful commercial uncooled thermal detector solutions rely heavily on technologies developed under the overall realm of Microelectromechanical Systems (MEMS) [1], [2], [4]–[7]. These include single detectors and focal plane arrays (FPAs) of thermopiles [8], bolometers [4], ferroelectric, and pyroelectric sensors [9]. The small size and low thermal mass of MEMS along with the ability to fabricate uniform arrays of identical sensors with a high yield makes this technology one of the most attractive choices.

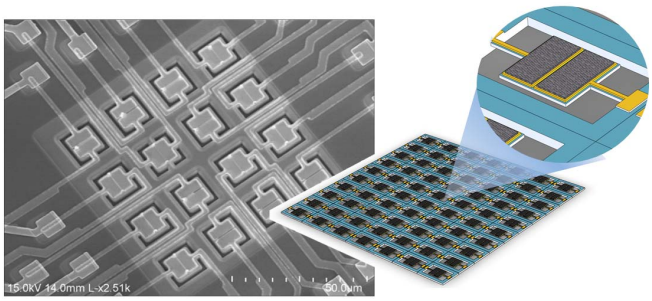

Fig. 1. A scanning electron microscope (SEM) image and a schematic of the micromechanical GaN resonators that can be used as highly sensitive, low-noise IR detectors.

A relatively unexplored technology for un-cooled IR sensors is the use of resonant detectors proposed by Vig *et al* [10], [11], who demonstrated micromachined quartz oscillators as the infrared sensing elements. According to this analysis, resonant IR detectors offer significant advantages in terms of the signal-to-noise ratio and sensitivity compared with other types of un-cooled detectors. The major practical challenges to this approach were associated with the difficulties of producing large arrays of identical mechanical elements [12], [13]. This problem, however, is specific to quartz since high-density micromachining on quartz substrates is difficult, if not impossible. With the current state of technology, it is possible to fabricate large densely packed arrays of resonators using other thin-film piezoelectric materials (Fig. 1).

We have previously demonstrated a high-sensitivity single micromechanical IR detector and reference pair made from thin-film gallium nitride (GaN) [14], [15]. In this work, we introduce small format arrays of GaN-based resonant detectors. Prototypes of these arrays are fabricated for preliminary testing and the measured results are presented. This is the first demonstration of resonant uncooled IR detector arrays based on thin-film micromechanical piezoelectric resonators.

II. Theory of Operation

The basic principle of transduction for a resonant IR detector is the change of its mechanical resonant frequency because of the temperature rise induced by the absorbed IR

Manuscript received September 25, 2013; revised November 13, 2013; accepted November 16, 2013. This work was supported in part by the National Science Foundation under Grant 1002036 and in part by the Army Research Laboratory under Contract W911NF. Subject Editor S. Merlo.

The authors are with the Department of Electrical Engineering and Computer Science, University of Michigan, Ann Arbor, MI 48109 USA (e-mail: vikrantg@umich.edu; minar@umich.edu).

Color versions of one or more of the figures in this paper are available online at http://ieeexplore.ieee.org.

Digital Object Identifier 10.1109/JMEMS.2013.2292368

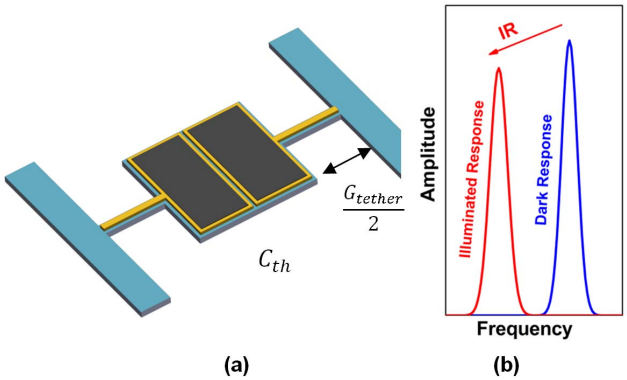

Fig. 2. (a) Each individual pixel in the array is a thin-film resonator mechanically suspended by thin tethers. The resonator body accounts for most of the thermal mass of the device, while the tethers isolate the resonator thermally. (b) The transduction mechanism depends on the change in the frequency of the resonator in proportion to the incident IR radiation.

radiation (Fig. 2). The mechanical resonator can be driven in an open loop or used in a self-sustaining oscillator by using simple and common feedback circuits, allowing continuous operation with a very stable frequency. Parametric changes to the resonator caused by heating are reflected as changes in the oscillator frequency. In this work, we focus on the design and analysis of the resonator as an IR sensing element. The resonant IR detector consists of a detector plate suspended by thin, high thermal resistivity tethers (Fig. 2). Different modes of resonance of the plate can be used for temperature sensing; here, we focus on the length extensional resonant mode. The resonance frequency is a function of temperature and is given by

$$f\,(T) = \frac{1}{2L\,(T)}\sqrt{\frac{C_{eff}\,(T)}{\rho_m}}, \tag{1}$$

where L, C_{eff}, and ρ_m are the length, effective stiffness, and mass density, respectively. The detector can be coated with a material that is an efficient thermal absorber of IR radiation. Commonly used materials such as silicon nitride, gold black, or experimental new materials such as nanocomposites can be used as IR absorbers [16]–[19]. The conversion of incident IR radiation power $\phi(\lambda)$ into temperature change is given by

$$\partial T = \frac{\eta(\lambda)\phi(\lambda)}{\sqrt{{G_{th}}^2 + {\omega_{ir}}^2 {C_{th}}^2}}, \tag{2}$$

where G_{th} is the effective thermal conductance of the device (dominated by the thermal conductance of the tethers), C_{th} is the thermal capacity of the device, ω_{ir} is the rate of change of the incident signal, and $\eta(\lambda)$ is the absorption efficiency of the IR absorber layer.

The relative change in resonator frequency is given by the temperature coefficient of frequency (TCF)

$$\alpha_T = \frac{1}{f(T)}\frac{\partial f}{\partial T}, \tag{3}$$

and is generally expressed in parts per million per K (ppm/K). The above equations allow us to translate the incident IR radiation power to a perceptible frequency shift.

In an array of resonant IR detectors, a small number of reference resonators can be included. These reference resonators will not have the IR absorber layer but have a top surface covered with metal electrodes that reflect ~99% of the incident IR radiation. In effect, this makes the reference resonator frequency invariant to IR heating, and allowing differential sensing in future implementations. This can potentially boost the system sensitivity, since the original beat frequency can be made extremely small, limited only by fabrication tolerances. Differential sensing also eliminates common-mode effects such as slow changes in ambient operating temperature, pressure variations in the sensor package, and acceleration. Differential measurements using beat frequency detection eliminate the need for a mechanical chopper, leading to savings in size, weight, and power.

III. Prototype Design & Fabrication

Important thermal parameters to consider while designing the resonator 'pixel' are the thermal conductance of the system and the thermal capacity of the body of the resonator, given by

$$G_{th} = G_{tethers} + G_{air} + G_{rad}, \tag{4}$$

and

$$C_{th} = \sum_i (\rho_m)_i \left(C_p\right)_i V_i \tag{5}$$

For a resonator made of multiple materials, including the piezoelectric film, the absorber, and metal electrodes, the thermal conductance through the tethers is given by:

$$G_{tethers} = 2\sum_i \frac{\kappa_i\,(A_t)_i}{(L_t)_i}. \tag{6}$$

for every i^{th} material in the composite stack. The quantities κ, ρ_m, C_p, A_t L_t, and V denote the thermal conductivity, mass density, specific thermal capacity, area of cross section of the tethers, length of tethers, and the volume of the resonator body. Note that the conductance doubles due to the presence of two tethers. The conductance through air and via radiation exchange (from both surfaces of the detector) is given by Eq. (7) and Eq. (8), respectively [20].

$$G_{air} = \frac{\kappa_{air} A}{d_{cavity}} \tag{7}$$

$$G_{rad} = 4(\varepsilon_{top} + \varepsilon_{bot})A\sigma_b T^3 \approx 8\varepsilon_D A\sigma_b T^3, \tag{8}$$

where κ_{air} and d_{cavity} are the thermal conductivity and height of the air column, A is the surface area of the detector, ε_{top} and ε_{bot} are the emissivity values of the top and bottom surfaces of the detector, σ_b is the Stefan-Boltzmann constant, and T is the absolute temperature of the detector. The conduction model through air is valid at measurement chamber pressure of about 20 μTorr. Estimated worst case scenario values for G_{air} and G_{rad} are 3.3×10^{-7} W/K and 7.8×10^{-8} W/K, respectively [20], which are negligible compared to the thermal conduction through the tethers for the present designs. The worst case scenario assumes the emissivity of the detector surface to be $\varepsilon_D = 1$, and κ_{air} of

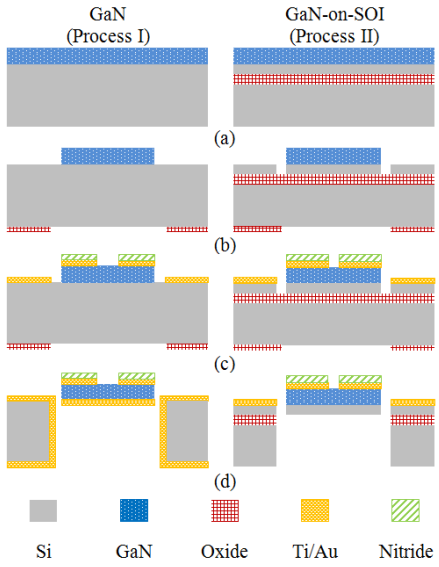

Fig. 3. Fabrication process flow for GaN (Process I) and GaN-on-SOI (Process II) resonators.

0.026 W/m-K [20], [21] (NIST specified value for atmospheric pressure at 300 K). The thermal time constant is defined as

$$\tau = C_{th} G_{th}^{-1}. \tag{9}$$

The thermal conductance can be engineered significantly using better design and low-conductivity materials. State-of-the-art bolometers have values of G_{th} on the order of 10^{-8} W/K, before being limited by radiation effects [22]. Such values of thermal conductance are possible for resonators with thinner films. Other feasible ways to decrease G_{th} is to use single tether designs or meandered tethers, while taking care to maintain good mechanical performance of the resonator.

The first prototype arrays fabricated consisted of resonators based on GaN and GaN-on-SOI thin films. The use of GaN-on-SOI wafers was necessitated by the low yield of this particular batch of thin-film GaN arrays due to high film stress. This problem can be solved by better control of the epitaxial growth of GaN, and has worked well in the past for fabricating high-performance GaN resonators on the order of 1 μm thickness [23]. Fig. 3 describes the fabrication process flow. GaN layer is grown on (111) silicon or SOI substrates using metallo-organic chemical vapor deposition (MOCVD). GaN wafers used in this work have been purchased from Nitronex Corp. [24]. More information about the epitaxial stack can be found in [24]. The resonator fabrication starts with defining the shape of the GaN resonator. The GaN layer was etched using inductively coupled plasma (ICP) with chlorine/boron chloride etching chemistry. For GaN-on-SOI resonators, the Si device layer is etched to the same lithographic pattern. The top electrode, consisting of Ti/Au, was patterned using evaporation and lift-off. A layer of silicon nitride was deposited and patterned on top of the electrodes as the IR absorber. Devices were released by selectively removing the silicon substrate from the backside using DRIE. Finally, the Ti/Au bottom electrode was sputtered from the backside. The GaN-on-SOI resonators do not need a bottom electrode as the Si layer is conductive enough to serve as the ground electrode.

TABLE I
MATERIAL PROPERTIES

Material	*Thermal Conductivity (W/m-K)*	*Mass Density (Kg/m^3)*	*Specific Heat capacity (J/kg-K)*
GaN	130	6150	490
Au	318	19300	129
Ti	22	4506	522
Si	130	2330	700
SiN_x	20	3100	700

TABLE II
GEOMETRY OF TETHERS AND RESONATOR BODY

Material	*Dimension*	*Tether Geometry*		*Resonator Plate Geometry*	
		GaN	**GaN-on-SOI**	**GaN**	**GaN-on-SOI**
		(µm)	**(µm)**	**(µm)**	**(µm)**
GaN	Length	30	30	80	80
	Width	5	5	80	80
	Thickness	1.425	1.425	1.425	1.425
Au	Length	30	30	75	75
	Width	3	3	77	77
	Thickness	0.2	0.1*	0.2	0.1*
Ti	Length	30	30	75	75
	Width	3	3	77	77
	Thickness	0.02	0.01*	0.02	0.01*
Si	Length	-	30	-	80
	Width	-	5	-	80
	Thickness	-	10	-	10
SiN_x	Length	-	-	60	60
	Width	-	-	74	74
	Thickness	-	-	0.2	0.2

*GaN-on-SOI resonators do not need a bottom metal electrode

TABLE III
CALCULATED THERMAL PERFORMANCE

Thermal Parameters	*units*	*GaN*	*GaN-on-SOI*
Total Conductance (both tethers)	W/K	7.45×10^{-5}	5.014×10^{-4}
Total Thermal Capacity	J/K	3.247×10^{-8}	1.353×10^{-7}
Thermal time Constant	ms	0.435	0.270

Tables I and II detail the material properties used in theoretical calculations and the geometries of the resonator and tethers. Table III describes the calculated values of the thermal properties of the resonators.

While the GaN arrays suffered from poor yield, the GaN-on-SOI arrays (Fig. 4(a)) had a near 100% process yield due to better mechanical stability. Further array measurements were therefore carried out on GaN-on-SOI arrays.

IV. MEASURED RESULTS

A. RF Performance

The nominal RF response of the GaN-on-SOI array is measured using an Agilent E5061 network analyzer with the appropriate calibration (Fig. 5). The resonators are driven at

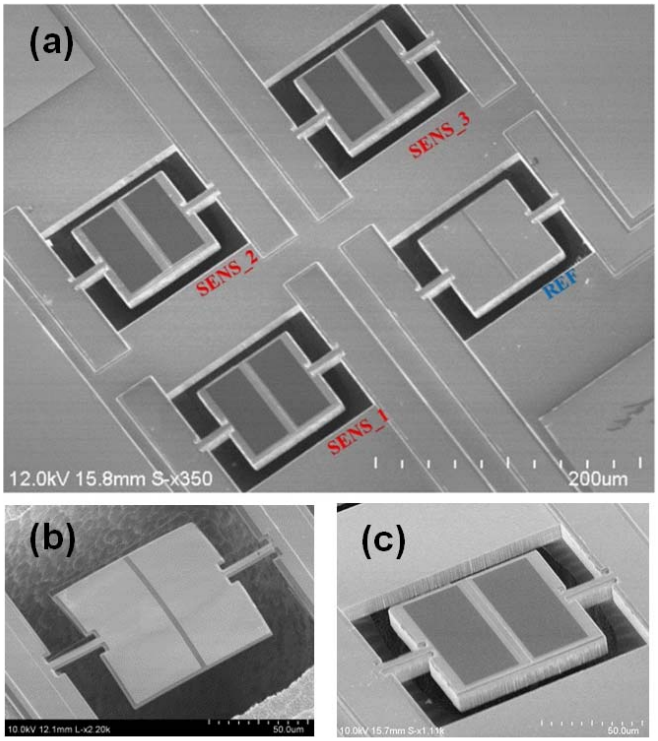

Fig. 4. (a) Fabricated array of GaN-on-SOI resonators. The three sensors and the single reference can be clearly differentiated by the presence or absence of the IR absorber layer. (b) A GaN reference resonator and (c) GaN-on-SOI sense resonator.

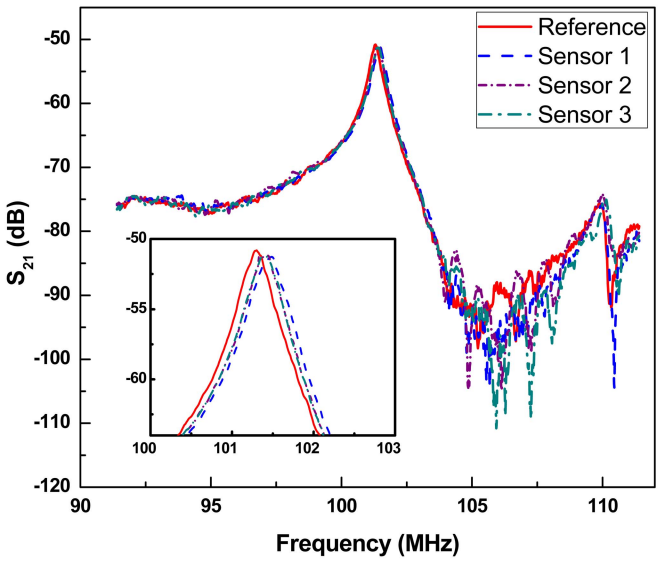

Fig. 5. Measured RF performance of the array shown in Fig. 4. The inset shows that the sense resonators are nearly identical while the reference resonator is only slightly different. The quality factor (Q) of the resonators in this array is ∼280 at 101 MHz. Significantly better Qs are possible and have been demonstrated previously using GaN resonators [23]. Measured results are obtained with 0 dBm RF power.

0 dBm, and allowed time to settle into a thermal equilibrium between the small level of drive induced heating and the ambient temperature. This self-heating is seen to be significant only at higher powers (+10 dBm or higher). The inset clearly shows that the three sense resonators are almost identical,

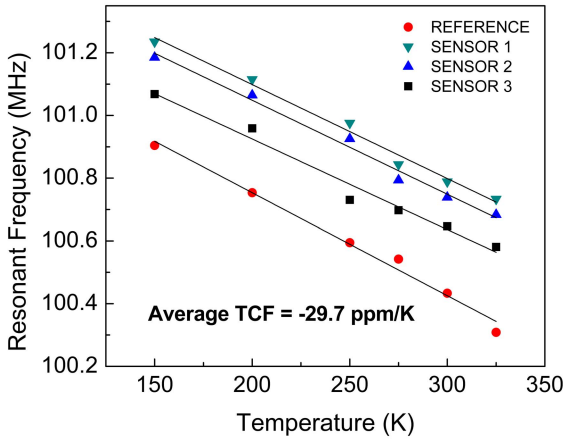

Fig. 6. The thermal dependence of the resonators in the array in the range from 150 K to 325 K. The TCF is calculated to be ∼ −29.7 ppm/K, indicating that the thermal performance is dominated by the thick Si layer.

while the reference resonator has a slightly different frequency because of the lack of the absorber layer and a different stress value in the resonating stack.

The value of α_T is extracted by measuring the frequency of the resonators at various temperatures (Fig. 6). Linear fitting of the data gives us an average α_T of −29.7 ppm/K. This value is close to the TCF of silicon, and we can conclude that the thermal response of these resonators is dominated by the TCF of the thick Si layer instead of the TCF of GaN [23], [25]–[28]. The use of GaN alone can be advantageous to this application, as its pyroelectric and electrostrictive properties can result in a large instantaneously induced frequency shift that can result in up to two orders of magnitude larger values of α_T [14], [29], [30]. However, to take advantage of this relatively unexplored effect, mechanical choppers are required. This approach is not the focus of the current work.

B. Infrared Response

The detectors are illuminated using an Ocean Optics near-IR Tungsten-Halogen lamp (HL2000-HP-FHSA) coupled into the probe station using (P400-1-VIS-NIR) optical fibers. The lamp has a power output of 20 W over the wavelength range of 360 nm - 2400 nm [31], while the optical fiber has a 92%-95% transmission in the wavelength range of 300 nm to 1100 nm (Fig. 7). Other wavelengths are assumed to be filtered out.

The array is measured in a Lakeshore cryogenic probe station with a controlled temperature and is shielded from external IR illumination. The NIR absorption of the silicon nitride absorber layer is characterized using a Perkin Elmer Spectrum-GX. Based on the radiation incident on the detector surface, and taking into account the measured NIR absorption characteristics of the silicon nitride absorber, we can calculate the radiation incident on the detector face to be 176 μW in the spectral range of 760 nm-1000 nm (boxed area of overlap in Fig. 7). This translates into a temperature shift of 70 mK. Given the 300 Hz frequency shift seen in the sensors (Fig. 8), this implies a radiant responsivity of 1.68%/W for the specified NIR spectral range. Due to the inherent difficulties in accurate

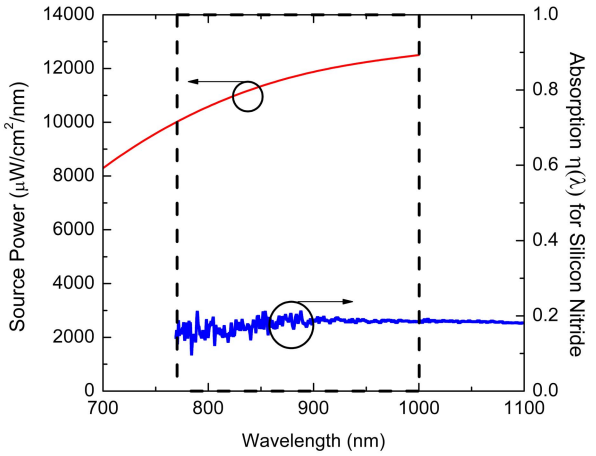

Fig. 7. The radiant power output of the source/optical fiber system as per vendor specifications [31], and the absorption efficiency of the silicon nitride layer, measured using NIR spectroscopy. The boxed area is the spectral region that describes the NIR radiation absorbed by the sense resonators.

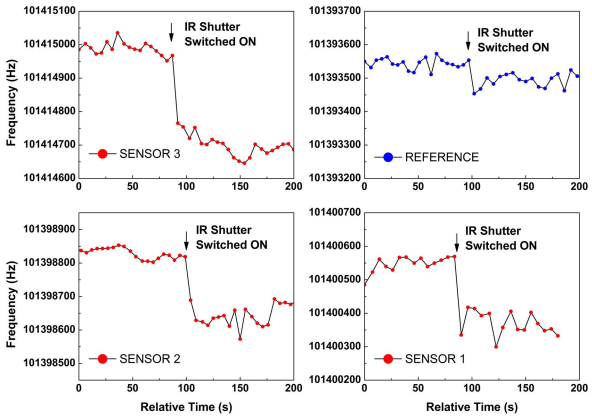

Fig. 8. Responses of all four resonators to near-IR illumination. The Y-axis span of all graphs is the same (500 Hz). The three sensors show ∼300 Hz decrease in frequency, while the reference exhibits very little shift. The long sampling time is due to the sweep speed of the network analyzer and is not the inherent thermal response of the resonators.

measurement of the irradiance at the detector surface without traceable blackbody calibration, at this point, we also estimate from the measured TCF that the temperature rise in the sensors is ∼100 mK. This difference can be accounted for by the fact that the system also absorbs slightly in the visible range, which is not taken into account in calculations due to lack of information about $\eta(\lambda)$ in that range.

It can be seen that the three sense resonators exhibit marked decreases of ∼300 Hz in their resonant frequencies upon IR illumination, while the reference resonator, while not perfectly invariant, has a significantly smaller frequency shift (Fig. 8). Better designs can amplify this difference by using higher TCF sense resonators and references that have smaller IR absorbance.

Based on the frequencies of the resonators in the array without any IR illumination (Fig. 9(a)), and the calculated beat frequencies upon subsequent IR illumination (Fig. 9(b)), we can see that even with a small increase in temperature due to

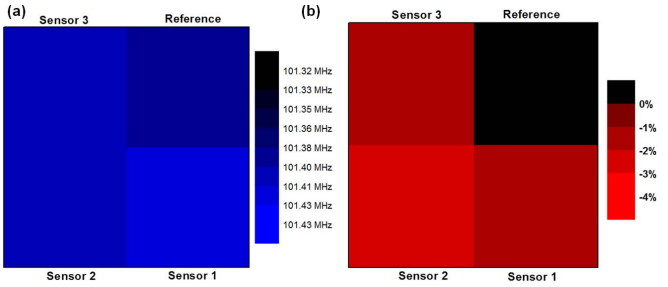

Fig. 9. (a) The frequencies of resonators in the array without IR illumination (dark response), (b) the relative change in beat frequencies of the sense resonators in the array upon IR illumination (IR response). The differential method imparts high sensitivity to IR radiation.

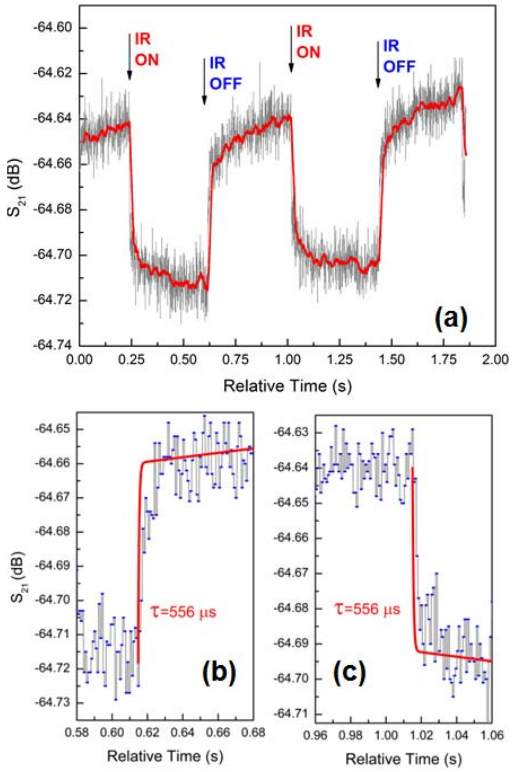

Fig. 10. (a) Transmission amplitude of the resonators under switched near-IR illumination. Measurements are acquired at high speeds to measure the resonator response shift upon illumination. Magnified ranges showing (b) cooling and (c) heating time constants based on measured data and curve fitting using double exponential functions to extract the thermal time constants. The slow time constant is due to the non-ideal substrate and surroundings, while the fast time constant (556 μs) is a function of the thermal properties of the sensors.

absorbed radiation, there is a significant relative change in the calculated beat frequency (between -1% and -2.5%) for an incident signal of 176 μW (or a temperature rise of 100 mK), leading to a high responsivity. Better characterization of the design and fabrication process can reduce the variation of the nominal beat frequencies and the IR response within the array.

C. Response Time

The thermal time constant of the resonators is critical in determining the measurement speed of the IR imager. For 30 Hz - 100 Hz operation, each resonator pixel should ideally

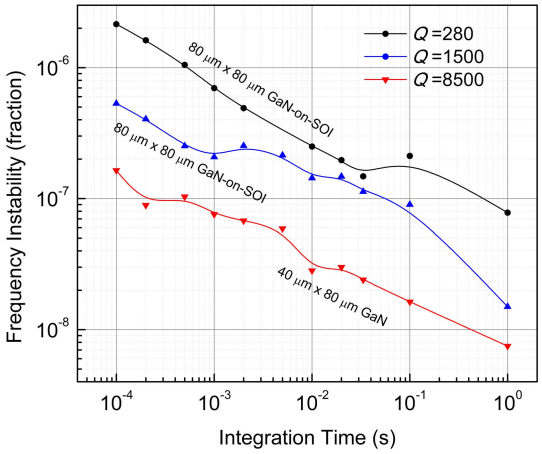

Fig. 11. Temporal frequency instability of the driven resonators at various integration times. The frequency instability is given by the ratio of the standard deviation to the average. Each point represents 128 continuous samples, with sample stage and radiation shield temperature maintained at 300 K ±10mK. Other resonators with higher values of Q are measured and validate the fact that it is possible to get lower instability values by improving Q. The best performance achieved was with a GaN resonator (Q = 8500) with frequency instability of 7.5 × 10^{-9} at 1 s integration time. This shows that it is possible to get very low frequency instability with the current approach.

have below 1 ms time constant. Thin film resonators are well suited for such fast responses due to their small thermal mass, as evidenced by the theoretical calculations for the two designs (Table III). Experimentally, the response time of the resonant IR detectors is characterized by measuring the rise or fall of the transmission signal level (S_{21}) with respect to switched IR illumination using a manual shutter. In order to ensure fast measurements of the thermal response, the device is stimulated using the network analyzer with a continuous wave (CW) signal with a fixed frequency f_{CW}. The choice of f_{CW} is based on preliminary frequency sweeps in order to identify the frequency at which the slope of S_{21} is the sharpest [32]. Data are captured using a fast integration bandwidth allowing for sampling at ∼20 μs intervals. Fig. 10(a) shows the measured response for a sense resonator over a few cycles of switched IR illumination. Fig. 10(b) and (c) show magnified regions of the response to illustrate the rise time and fall time for the detector. Two distinct time constants can be extracted: for the heating/cooling of the device, and the heating/cooling of the surrounding regions of the substrate and measurement chamber [13]. The time constants of the device and the substrate can be estimated from curve fitting of the data using a double exponential fit to be approximately 556 μs, and 1000 s, respectively. The measured time constant is in the same order as the calculated value; however, a better measurement setup should be used to get a more accurate estimate of the time response and close the gap between measurement and calculations.

D. Short Term Frequency Instability

The temporal noise of each detector pixel can be characterized by the short term frequency instability, defined as the ratio of the standard deviation and the average value of a small set of continuous data samples [13] (Fig. 11). Care must be taken to ensure that the characterization conditions eliminate noise from external sources as far as possible. The devices measured here are measured in a stable vacuum (10-17 μTorr) and in a temperature controlled, radiation shielded (dark) chamber. The temperatures of the stage and the walls of the chamber are monitored synchronously and maintained at 300 K ±10mK. This ensures that the pressure and thermal fluctuation noise is minimized. As expected, the frequency instability is lower with higher integration time. We also measure other resonators (not from the same array) with higher values of Q to experimentally verify that improved Q will result in significantly lower frequency instability. A GaN resonator with a Q of 8500 demonstrated the lowest frequency instability of 7.5 × 10^{-9} with an integration time of 1 s.

V. Design for Low NETD

An important metric for IR detectors is the noise equivalent temperature difference (NETD). State-of-the-art uncooled detectors demonstrate measured NETD values between 30 mK to 50 mK [7]. The NEDT can further be decomposed into spatial and temporal components [33]. For resonant IR detectors, the analytical model for temporal thermal NETD is given by [10]

$$NETD = \frac{\left(4F^2+1\right)\sigma_N}{\tau_{opt}\beta A\Re}\left[\left(\frac{\Delta P}{\Delta T}\right)_{\lambda_1-\lambda_2}\right]^{-1}, \qquad (10)$$

where F is the focal ratio of the focusing optics, τ_{opt} is the transmissivity of the focusing optics, β and A are the fill factor and area of the resonator, and σ_N is the frequency instability. $\Re$ is the responsivity (in terms of incident power radiated by a blackbody source), $\left(\frac{\Delta P}{\Delta T}\right)_{\lambda_1-\lambda_2}$. $\Re$ is the change in power per unit area per temperature increase measured within the given spectral band λ_1 to λ_2, and is expressed as [10]

$$\Re\left(\omega_{ir}\right) = \frac{\eta(\alpha_T)}{G_{th}\sqrt{\left(1+\omega_{ir}^2\tau^2\right)}}. \qquad (11)$$

As expected there will need to be a tradeoff between responsivity and frequency instability. We can combine Eq. (10) and Eq. (11) to expand the relation for NETD in terms of all the operating parameters as follows.

$$NETD = \frac{\left(4F^2+1\right)\sigma_N G_{th}\sqrt{\left(1+\omega_{ir}^2\tau^2\right)}}{\tau_{opt}\beta A\eta(\alpha_T)}\left[\left(\frac{\Delta P}{\Delta T}\right)_{\lambda_1-\lambda_2}\right]^{-1}. \qquad (12)$$

The critical design parameters here are the thermal conductance, frequency instability and the TCF. The most important design range is the long wavelength IR (LWIR). Based on the present measured results, we can make some assumptions with a view towards setting achievable goals for low thermal NETD in the future. Improved absorbing materials can potentially give us up to 90% absorption over a broad spectral range [16]–[19]. Further, better design and fabrication can achieve lower values of frequency instability. Of the noise processes that could affect the micromechanical resonator frequency significantly, the dominant source is the temperature fluctuation induced frequency instability [10], [34]. Theoretically,

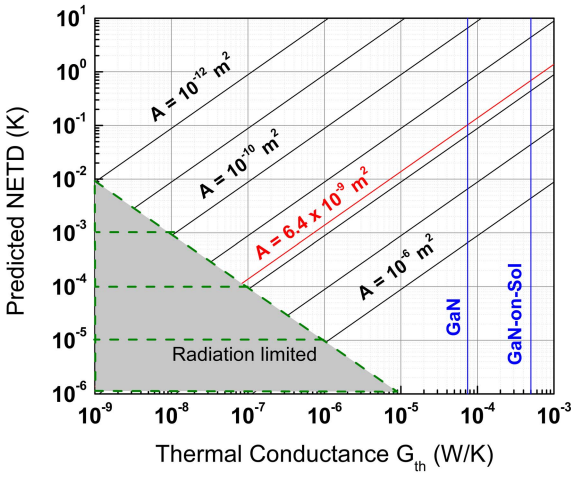

Fig. 12. Predicted values of temporal NETD for the resonator pixel as a function of thermal conductance, using the model and assumptions described in Section V. Calculated NETD values for the fabricated devices and the radiation limits are marked.

for room temperature conditions, and assuming conservative values of resonator Q and input power levels, the limiting value for total short-term frequency noise can be estimated to be on the order of 10^{-11} [34], [35]. Practical MEMS oscillators have been able to achieve measured short-term frequency stabilities between 5×10^{-9} [36] and 6×10^{-10} [37], with larger resonators, and the design optimization challenge will be to reach these values while maintaining the small footprint and thermal mass required for IR detectors. As seen in the measured results above and prior literature [34], [35], frequency instability scales inversely with the loaded Q. Values for Q on the order of 10^4 in the frequency range of 1 MHz – 1 GHz using thin-film piezoelectric materials have been measured practically [23], [26], [38]. Higher Qs also improve the sensing resolution as the minimum detectable frequency shift for mechanical resonators scales inversely with $\sqrt{Q}$ [39].

Based on our measured results we can predict the expected thermal NETD goal in the LWIR regime with some optimistic assumptions for σ_N and $\eta(\lambda)$. Fig. 12 depicts the temporal NETD as a function of thermal conductance and area (from Eq. (12)) assuming $\sigma_N = 10^{-10}$, $|\alpha_T| = 30$ ppm/K and $\eta(\lambda) = 0.9$. Fig. 12 also indicates the calculated performance of the fabricated GaN and GaN-on-SOI resonators. The GaN (GaN-on-SOI) resonator can achieve 102 mK (690 mK) temporal NETD, with the given assumptions. It is apparent that while the NETD performance of these prototypes is not yet comparable to state-of-the-art bolometers [7], there is a pathway towards smaller thermal NETD values using MEMS resonators. The radiation limit as a function of the detector area is indicated on the plot. Based on Fig. 12, possible ways to decrease NETD of the resonator pixels is to reduce the thermal conductivity of the tethers using thinner GaN films or other low thermal conductivity materials, using single tether designs, increasing fill factor, and using more efficient IR absorbers. These approaches are currently being explored.

The spatial noise in the system is not easily modeled analytically and is a function of the fabrication tolerances that allows very precise nominal performance, as well as the spatial variation in the responsivity of the pixel array. Initial results shown here (Fig. 9) indicate that it possible to get reasonably precise performance, however, more exhaustive studies are necessary on much larger arrays before strong assertions can be made. Fixed-pattern spatial noise can be mitigated or eliminated during signal processing [33]. Structural solutions such as oxide trenches that provide pixel isolation can be explored to mitigate the spatial noise due to cross-coupling between pixels. Furthermore, it is possible to use an array of resonators with slightly varying planar dimensions (and thus frequencies) [10]. The highly precise frequencies and narrow bandwidths afforded by mechanical resonators can allow frequency division multiplexing (FDM) of entire rows/columns of resonators on a single signal line, and reduce spatial noise.

VI. Conclusion

This work demonstrates the first experimental prototype arrays of mechanically resonant IR detectors using thin-film piezoelectric materials that convert incident IR radiation into large relative shifts in frequency that can be sensed electronically. Using a reference resonator, we can achieve an average of -1.5 % shift in beat frequency for a 100 mK temperature rise. The small resonators have a fast time constant of 556 μs, and a frequency instability on the order of 10^{-6}.

While significant improvements in design and testing methodology are necessary for the practical validation of this concept, thin-film piezoelectric resonators can make it possible to design and fabricate medium and large scale arrays that can possibly compete with existing IR imager technologies. The present work has focused on arrays with small pixel size in order to conform to industry norms for IR imagers. However the same design principles and analyses are valid for larger and slower resonant detectors that can provide higher sensitivity and significantly lower noise. Such resonators can be used as single element detectors (industrial sensors) or for small format imaging cores for IR telescopes, where the emphasis is not on size/speed, but on sensitivity.

Acknowledgment

The authors thank the staff at the Lurie Nanofabrication Facility, University of Michigan, Ann Arbor, MI, USA for providing fabrication facilities and support and the staff at the Analytical Instruments Laboratory at the Department of Chemistry for their help with spectroscopy measurements.

References

[1] P. W. Kruse, *Uncooled Thermal Imaging : Arrays, Systems, and Applications*. Bellingham, WA, USA: SPIE Press, 2001.
[2] A. Rogalski, "Infrared detectors: Status and trends," *Progr. Quantum Electron.*, vol. 27, no. 2, pp. 59–210, 2003.
[3] L. Becker, "Influence of IR sensor technology on the military and civil defense," *Proc. SPIE*, vol. 6127, pp. 61270–61278, Feb. 2006.
[4] R. A. Wood, "Monolithic silicon microbolometer arrays," in *Semiconductors and Semimetals*, vol. 47, W. K. Paul and D. S. David, Eds., New York, NY, USA: Elsevier, 1997, pp. 43–121.
[5] F. Niklaus, C. Vieider, and H. Jakobsen, "MEMS-based uncooled infrared bolometer arrays: A review," *Proc. SPIE*, vol. 6836, pp. 68360D–68364D, Jan. 2007.

[6] P. R. Norton, "Infrared detectors in the next millennium," *Proc. SPIE*, vol. 3698, pp. 652–665, Jun. 1999.
[7] A. Rogalski, "Infrared detectors for the future," *Acta Phys. Polonica-Ser. A General Phys.*, vol. 116, pp. 389–395, Feb. 2009.
[8] A. D. Oliver and K. D. Wise, "A 1024-element bulk-micromachined thermopile infrared imaging array," *Sens. Actuators A, Phys.*, vol. 73, no. 3, pp. 222–231, 1999.
[9] P. Muralt, "Micromachined infrared detectors based on pyroelectric thin films," *Rep. Progr. Phys.*, vol. 64, no. 10, pp. 1339–1343, 2001.
[10] J. R. Vig, R. L. Filler, and Y. Kim, "Microresonator sensor arrays," in *Proc. IEEE Freq. Control Symp.*, Jun. 1995, pp. 852–869.
[11] J. R. Vig, R. L. Filler, and K. Yoonkee, "Uncooled IR imaging array based on quartz microresonators," *J. Microelectromech. Syst.*, vol. 5, no. 2, pp. 131–137, 1996.
[12] Y. Kim and J. R. Vig, "Experimental results on a quartz microresonator IR sensor," in *Proc. IEEE Ultrason. Symp.*, Oct. 1997, pp. 449–453.
[13] P. Kao and S. Tadigadapa, "Micromachined quartz resonator based infrared detector array," *Sens. Actuators A, Phys.*, vol. 149, pp. 189–192, Feb. 2009.
[14] V. J. Gokhale and M. Rais-Zadeh, "Sensitive uncooled IR detectors using gallium nitride resonators and silicon nitride absorbers," in *Proc. Solid-State Sensors, Actuat. Microsyst. Workshop*, 2012, pp. 1–4.
[15] V. J. Gokhale, Y. Sui, and M. Rais-Zadeh, "Novel uncooled detector based on gallium nitride micromechanical resonators," *Proc. SPIE*, vol. 8353, pp. 835319-1–835319-3, May 2012.
[16] Y. Sui, V. J. Gokhale, O. A. Shenderova, G. G. McGuire, and M. Rais-Zadeh, "A thin-film infrared absorber using CNT/nanodiamond nanocomposite," in *Proc. MRS*, 2012, pp. 1–6.
[17] V. J. Gokhale, O. A. Shenderova, G. E. McGuire, and M. Rais-Zadeh, "Infrared absorption properties of carbon nanotube/nanodiamond based thin film coatings," *J. Microelectromech. Syst.*, to be published, DOI: 10.1109/JMEMS.2013.2266411.
[18] K. Mizuno, J. Ishii, H. Kishida, Y. Hayamizu, S. Yasuda, D. N. Futaba, *et al.*, "A black body absorber from vertically aligned single-walled carbon nanotubes," *Proc. Nat. Acad. Sci. United States Amer.*, vol. 106, pp. 6044–6047, Apr. 2009.
[19] J. Lehman, E. Theocharous, G. Eppeldauer, and C. Pannell, "Gold-black coatings for freestanding pyroelectric detectors," *Meas. Sci. Techol.*, vol. 14, pp. 916–922, Jul. 2003.
[20] M. Liger, "Uncooled carbon microbolometer imager," Ph.D. dissertation, Dept. Eng. Appl. Sci., California Inst. Technol., Pasadena, CA, USA, 2006.
[21] K. Stephan and A. Laesecke, "The thermal conductivity of fluid air," *J. Phys. Chem. Ref. Data*, vol. 14, no. 1, pp. 227–234, 1985.
[22] M. Kohin and N. R. Butler, "Performance limits of uncooled VO_x microbolometer focal plane arrays," *Proc. SPIE*, vol. 5406, pp. 447–453, Apr. 2004.
[23] V. J. Gokhale, J. Roberts, and M. Rais-Zadeh, "High performance bulk mode gallium nitride resonators and filters," in *Proc. 16th Int. Solid-State Sensors, Actuat. Microsyst. Conf.*, 2011, pp. 926–929.
[24] Nitronex Corp., Durham, NC, USA. (2013) [Online]. Available: http://nitronex.com/
[25] A. Ansari, V. J. Gokhale, V. A. Thakar, J. Roberts, and M. Rais-Zadeh, "Gallium nitride-on-silicon micromechanical overtone resonators and filters," in *Proc. IEEE IEDM*, Dec. 2011, pp. 1–4.
[26] G. Piazza, P. J. Stephanou, and A. P. Pisano, "Piezoelectric aluminum nitride vibrating contour-mode MEMS resonators," *J. Microelectromech. Syst.*, vol. 15, pp. 1406–1418, Dec. 2006.
[27] A. K. Samarao and F. Ayazi, "Temperature Compensation of silicon resonators via degenerate doping," *IEEE Trans. Electron Devices*, vol. 59, no. 1, pp. 87–93, Jan. 2012.
[28] V. A. Thakar, Z. Wu, A. Peczalski, and M. Rais-Zadeh, "Piezoelectrically transduced temperature-compensated flexural-mode silicon resonators," *J. Microelectromech. Syst.*, vol. 22, pp. 815–823, Jun. 2013.
[29] M. Willatzen, L. Wang, and L. C. Lew Yan Voon, "Electrostriction in GaN/AlN heterostructures," *Superlattices Microstruct.*, vol. 43, nos. 5–6, pp. 436–440, 2008.
[30] M. Willatzen and L. C. Lew Yan Voon, "Static and dynamic effects due to electrostriction in GaN/AlN," *J. Phys., Condens. Matter*, vol. 19, no. 50, pp. 506202-1–506202-3, 2007.
[31] (2000). *Ocean Optics HL-2000* [Online]. Available: http://www.oceanoptics.com/products/hl2000.asp
[32] Y. Hui and M. Rinaldi, "Fast and high resolution thermal detector based on an aluminum nitride piezoelectric microelectromechanical resonator with an integrated suspended heat absorbing element," *Appl. Phys. Lett.*, vol. 102, pp. 093501-1–093501-4, Mar. 2013.
[33] R. G. Driggers, "Noise equivalent temperature difference," in *Encyclopedia of Optical Engineering*, vol. 2, Cleveland, OH, USA: CRC Press, 2006, pp. 1470–1472.
[34] A. N. Cleland and M. L. Roukes, "Noise processes in nanomechanical resonators," *J. Appl. Phys.*, vol. 92, pp. 2758–2769, Sep. 2002.
[35] F. L. Walls and J. R. Vig, "Fundamental limits on the frequency stabilities of crystal-oscillators," *IEEE Trans. Ultrason. Ferroelectr. Freq. Control*, vol. 42, no. 4, pp. 576–589, Jul. 1995.
[36] H. J. Lee, K. K. Park, P. Cristman, O. Oralkan, M. Kupnik, and B. T. Khuri-Yakub, "A low-noise oscillator based on a multi-membrane CMUT for high sensitivity resonant chemical sensors," in *Proc. IEEE Micro Electro Mech. Syst.*, Jan. 2009, pp. 761–764.
[37] J. E. Y. Lee, B. Bahreyni, Z. Yong, and A. A. Seshia, "A single-crystal-silicon bulk-acoustic-mode microresonator oscillator," *IEEE Electron Device Lett.*, vol. 29, no. 7, pp. 701–703, Jul. 2008.
[38] R. Tabrizian, M. Rais-Zadeh, and F. Ayazi, "Effect of phonon interactions on limiting the f.Q product of micromechanical resonators," in *Proc. Int. Solid-State Sensors, Actuat. Microsyst. Conf.*, 2009, pp. 2131–2134.
[39] T. R. Albrecht, P. Grutter, D. Horne, and D. Rugar, "Frequency-modulation detection using high-Q cantilevers for enhanced force microscope sensitivity," *J. Appl. Phys.*, vol. 69, pp. 668–673, Jan. 1991.

Vikrant J. Gokhale (S'10) received the B.Tech. degree in electronics and instrumentation engineering from the Vellore Institute of Technology, Tamil Nadu, India, and the M.S. degree in electrical and computer engineering from the University of Michigan, Ann Arbor, in 2007 and 2010 respectively. He is currently a doctoral candidate in electrical engineering at the University of Michigan, Ann Arbor. From 2007 to 2008, he worked as an Engineer at Honeywell Technology Solutions, Sensing and Control, Bangalore, India. His research interests include MEMS sensor design and fabrication, GaN resonators, resonant infrared detectors, carbon nanotube based nanocomposites, and the acoustoelectric effect in piezoelectric semiconductor materials.

Mina Rais-Zadeh (S'03–M'08–SM'12) received the B.S. degree in electrical engineering from Sharif University of Technology and M.S. and Ph.D. degrees both in Electrical and Computer Engineering from Georgia Institute of Technology in 2005 and 2008, respectively. From August 2008 to 2009, she was a Postdoctoral Research Fellow with the Integrated MEMS Group, Georgia Institute of Technology. Since January 2009, she has been with the University of Michigan, Ann Arbor, where she is currently an Assistant Professor in the Department of Electrical Engineering and Computer Science. Dr. Rais-Zadeh is the recipient of the NSF CAREER Award (2011), IEEE Electron Device Society Early Career Award (2011), and the NASA Early Career Faculty Award (2012). She was the finalist in student paper competitions at the SiRF (2007) and IMS (2011) conferences. She is the chairperson of the Display, Sensors and MEMS (DSM) sub-committee at the 2013 IEEE International Electron Devices Meeting (IEDM) and a senior member of IEEE. She has served as a member of the technical program committee of IEEE IEDM, IEEE Sensors Conference, and the Hilton Head workshop. Her research interests include RF MEMS, passive micromachined devices for communication applications, resonant micromechanical devices, gallium nitride MEMS, and micro/nano fabrication process development.